AIAA JOURNAL
Vol. 45, No. 9, September 2007

Numerical Simulation of Octogen-Based Propellant

L. Massa* and T. L. Jackson†
University of Illinois at Urbana–Champaign, Urbana, Illinois 61801
and
J. D. Buckmaster‡
Buckmaster Research, Urbana, Illinois 61801

DOI: 10.2514/1.27852

In this paper, we present a set of computational simulations of the deflagration of composite propellants comprising octogen and hydroxyl-terminated polybutadiene. The focus of the investigation is on the parameter calibration of simplified global kinetics models used to determine gas-phase chemical rates. The calibration is based on a collection of experimentally measured burning characteristics for pseudopropellants comprising octogen and hydroxyl-terminated polybutadiene with different solid loadings and uses exclusively homogeneous, one-dimensional, steady burning information. The task of including a large set of burning characteristics is accomplished by transforming the calibration into an optimization problem that is solved by means of a genetic algorithm. Models of increasing accuracy are constructed by enlarging the set of matched performance and the parameter space. The objective is to demonstrate the influence of the calibration of such models on three-dimensional simulations in which the size of the oxidizer particles is not neglected. A quantitative comparison of prediction and experiments is presented.

Nomenclature

A_p	=	preexponential term in the burn-rate power law
A_{pl}	=	preexponential term in the scaled burn-rate power law
a_λ	=	parameter in the thermal conductivity equation
b_λ	=	parameter in the thermal conductivity equation
c_p	=	specific heat at constant pressure
$D_{g,i}$	=	preexponential terms of gaseous chemical reactions
D_s	=	preexponential term of pyrolysis law
e_λ	=	temperature exponential in the thermal conductivity equation
$\mathcal{F}$	=	fitness function of the optimization algorithm
g	=	normal component of the temperature gradient at the solid side of the burning interface
Le	=	Lewis number
m_i	=	temperature exponents in gaseous reaction terms
N_m	=	number of matching conditions in the optimization
N_r	=	number of reactions
N_s	=	number of species
n_i	=	pressure exponents in gaseous reaction terms
n_p	=	pressure exponent in the burn-rate power law
n_{pl}	=	pressure exponent in the scaled burn-rate power law
n^*	=	pressure-exponent scale in the scaled burn-rate power law
P	=	pressure
p^*	=	pressure scale in the scaled burn-rate power law
Q	=	heat release in the solid phase
R_p	=	pressure response
r_b	=	burn rate
T	=	temperature
V_b	=	vector of measured (target) burning characteristics, size N_m
V_p	=	vector of predicted burning characteristics, size N_m
Y	=	species mass fractions
α_i	=	energy conservation coefficients
α_s	=	thermal diffusivity in the solid phase
$\beta_{i,k}$	=	mass conservation coefficients
ζ	=	stability parameter
Θ	=	scaled activation temperature in pyrolysis law
θ	=	scaled activation temperature in gaseous reaction terms
λ	=	thermal conductivity coefficient
μ	=	pressure exponent in pyrolysis law
$\nu_{i,k}$	=	mass fraction exponents in gaseous reaction terms
ρ	=	mass density
σ	=	supply-temperature burn-rate sensitivity

Subscripts

blend	=	fine blend of hydroxyl-terminated polybutadiene and octogen within the solid phase
g	=	gas phase
hmx	=	octogen particles within the solid phase
htpb	=	hydroxyl-terminated-polybutadiene matrix within the solid phase
s	=	solid phase

Received 16 September 2006; revision received 6 April 2007; accepted for publication 10 April 2007.

*Research Scientist, Center for Simulation of Advanced Rockets; currently Department of Mechanical Engineering, Clemson University; lmassa@clemson.edu. Member AIAA.

†Senior Research Scientist, Center for Simulation of Advanced Rockets; tlj@csar.uiuc.edu. Associate Fellow AIAA.

‡2014 Boudreau; limey@uiuc.edu. Associate Fellow AIAA.

I. Introduction

SOLID propellants most often comprise a heterogeneous composite material, built as a dispersion of discrete particles of oxidizer in a fuel-binder matrix. The particle size distribution influences the deflagration process and the combustion field supported by the propellant. The interaction between the particle morphology and the rocket chamber system is of interest for a number of reasons. Burn-rate control is an obvious one: The particle size is often used to modify the slope of the burn rate vs pressure curve in rocket motor applications. Another way in which solid-phase heterogeneity influences the chamber flow is by rendering the propellant efflux a stochastic random field. The interaction between the stochastic efflux and the turbulent flowfield supported by the burning propellant is the subject of the computational investigation of Massa et al. [1]. Validation and improvement of combustion models used in computer simulations is critical to the effectiveness of

numerical methods in exploring the complex rocket chamber flow system.

The present investigation has two primary objectives. The first objective is to explore the accuracy of 3-D computational simulations of octogen (HMX)-based heterogeneous propellant deflagration. A computational framework for the simulation of randomly packed propellant was developed by Jackson and Buckmaster [2] and was successfully applied to simulate the burning of ammonium-perchlorate (AP)-based propellant. A propellant mix of AP and hydroxyl-terminated polybutadiene (HTPB), the backbone of most solid rocket motor propellants, supports a moderately corrugated regressing surface and a smooth deflagration process. Conversely, experimental observations described by Beckstead and McCarty [3] suggest that HMX–HTPB oxidizer–fuel mixes are characterized by a highly corrugated solid-gas interface and an intermittent burning process. Both of these features result in an irregular deflagration and considerably complicate the computational analysis.

The second objective is to present an analysis of reaction schemes for solid-propellant deflagration and to introduce a modeling strategy that relies primarily on optimization of an objective cost function. The issue of kinetic modeling arises due to the very complex nature of the chemistry involved in the process. A first principle model of solid-propellant combustion should include a solid phase in which chemical reactions are scarce, a condensed multicomponent interface (solid, liquid, or gas), and a gas phase. Of these phases, only the first and last are (in some cases, mostly one-dimensional problems) appropriately modeled from first principle. The major difficulty in modeling condensed-phase reaction paths is caused by the fact that the kinetic rates do not generally obey order-n Arrhenius laws. Therefore, model-free methods such as isoconversional methods have been devised to overcome this obstacle (Vyazovkin and Wight [4]). Although great progress has been made in studying the gas-phase reactions, the weakest link is the condensed layer, in which a considerable amount of the heat of explosion is released. For example, Miller and Anderson [5], analyzing HMX deflagration, pointed out that the gas-phase temperature and species-mass-fraction profiles can be obtained with a comparable level of accuracy by considering totally different reaction paths in the solid phase and by modeling the gas phase with detailed kinetics. Brewster [6] pointed out that a simple chemistry model based on a single global kinetic path in the gas phase yields a better agreement than a detailed kinetics model in predicting the pressure-coupled response function of HMX.

In addition to issues of uncertainty in the model assumptions, practical issues (e.g., high computational run time and lack of robustness) make detailed kinetics models unsuitable for three-dimensional computer simulations of heterogeneous propellant combustion. Therefore, 3-D computations are most often carried out with simplified kinetic schemes that can be either reduced schemes or global (false) schemes. The advantage of the first choice is the higher degree of representation of the underlying physics, whereas the second choice requires less detailed information about the chemistry and yields, in general, simpler formalisms.

Global schemes can be appropriately calibrated to yield predictions that are as accurate as needed by enlarging the parameter space. However, these predictions are limited to only global performance variables; therefore, the success of the model when applied to problems other than those for which it was calibrated is not guaranteed. Another drawback of global schemes is reflected in the question: "How does one choose the model parameters when using global kinetics?" We advocate using numerical optimization. The use of numerical optimization to determine the model parameters is a consequence of two considerations. First, the kinetic parameters for a global kinetic scheme do not have a direct physical interpretation, and so the calibration can only be defined as the calibration that gives the best match for a set of global performance variables. Second, the scatter in experimental data makes it impossible to define a model by exactly matching a subset of performance variables, and so the definition of a least-squares type of function is a natural choice.

A calibration procedure based on numerical optimization is applicable to a large class of solid energetic materials. The approach is discussed by Massa et al. [7], in which the calibration strategy is illustrated by considering AP- and HMX-based propellants. In this research, we restrict our attention to modeling HMX–HTPB propellants and the emphasis is on the accuracy of the optimized models when applied to 3-D-supported deflagrations. Three models of increasing complexity are developed, and the ability of such models to predict 3-D burn-rate data is linked to the number of parameters and objective targets used in the 1-D calibration.

The present manuscript is organized as follows: Sec. II contains a review of global kinetic modeling in solid propellants, Sec. III introduces the reaction formalism used in this research, Sec. IV lists optimized models for different calibration conditions, Sec. V gives detailed information about the 3-D analysis, Sec. VI details computational results for two morphologies, and Sec. VII presents the conclusions to this investigation.

II. Global Kinetics Models

In the context of global kinetics, it is necessary to recognize that some of the model parameters have weak physical meaning and seldom can they be chosen based upon experiments. Global kinetics are based on a phenomenological description of the combustion process, one in which each flame (i.e., region of high chemical energy release) is associated with an Arrhenius reaction term that describes a very complex set of chemical reactions.

A large number of global schemes for solid-propellant deflagration have been proposed since Second World War; a critical review is given by Miller [8]. For pure HMX, we reference the works of Ben-Reuven and Caveny [9], Ward et al. [10], and Mitani and Williams [11]. All of these models yield good quantitative predictions, but with quite different parameter selections.

The accuracy of the model is related to the choice of performance used to quantify the agreement between the computational model and experiments. The engineering practice led to the description of solid-propellant deflagration based upon a set of performance measurements that includes, but is not limited to, steady-state burn rates for different pressures, adiabatic flame temperatures, sensitivity derivatives, intrinsic stability information, and pressure-response data. In the present manuscript, this set of quantitative measurements comprises what we shall call burning characteristics. An appropriate global kinetics model should be able to reproduce observed trends for most of the burning characteristics. Therefore, the two fundamental issues in global kinetics modeling are accuracy and uniqueness or, in another words, how the best model can be chosen given a set of conditions.

A. Global Optimization

The requirements of accuracy and uniqueness identify the model as the optimal choice for a subset of the burning characteristics, thus transforming the calibration into an optimization problem. A global optimization point is unique and leads by definition to the best possible agreement with target values. A similar approach was used by Price et al. [12], who proposed defining uncertain model parameters based on those that minimize an objective function.

The approach advocated here requires the definition of a scalar objective function defined on the parameter space and a set of inequalities that define the boundary of such parameter space. The objective function needs to be large enough to contain information about all of the important burning characteristics of the propellant. The optimal parameters are then determined by using a genetic optimization algorithm to search for the function's global maximum within the parameter space.

A parallel genetic algorithm takes advantage of the intrinsic independence of random-search-algorithm function evaluations, thus exploiting computation concurrence in a distributed-memory parallel-computing environment. The reduced run time of the message-passing-interface version of the genetic algorithm allows optimizations of models with a very large number of parameters and target burning characteristics. A fundamental problem of our approach, based exclusively on a cost-function minimization, is the tendency to obtain models that lead to nonphysical behavior. This

drawback can be overcome by increasing the number of model parameters and target burning characteristics. The size of the burning characteristics set is often limited by the availability of experimental data. When neither the parameter nor the target space can be increased, appropriate bounds on the model variables can be imposed to avoid nonphysical results. Thus, the optimization is unique once the number of parameters and the bounds have been set. Note that we use only 1-D information in calibrating the combustion model; the 3-D experimental data are reserved for validation.

The set of one-dimensional burning characteristics considers both pure-HMX and HMX–HTPB pseudopropellants of different solid loadings. The word pseudopropellant is used to describe an ideal mix of fuel and oxidizer, in which the particle sizes are small compared with all of the other physical length scales, and so the material can be considered homogeneous and supportive of premixed combustion.

Different models that are 1-D optimal for the underlying set of parameters and bounds are considered. The models are tested with respect to their ability to produce multidimensional burning characteristics in agreement with the experiments.

B. Genetic Algorithm

The algorithm is described in greater detail by Massa et al. [7]. The fitness function (i.e., the function that is maximized in the random search) is taken to be the inverse of the sum of the squares of the error between predicted 1-D burning characteristics and experimental measurements. By assembling the target and predicted burning characteristics into column vectors of length N_m, V_b, and V_p, respectively, and defining the ratio vector as

$$r = [(V_b/V_p)_1, (V_b/V_p)_2, \ldots, (V_b/V_p)_{N_m-1}, (V_b/V_p)_{N_m}]^T$$

the fitness function can be simply written as

$$\mathcal{F} = [(r-1)^T(r-1)]^{-1} \tag{1}$$

Optimization through a genetic algorithm does not require the evaluation of gradients of the fitness function to find its global maximum. Nevertheless, the application of the technique to solid-propellant modeling requires the evaluation of solution sensitivity derivatives as part of the definition of the objective function (cf. Sec. II). Evaluation of sensitivity derivatives involves the exact determination of the Jacobian of the algebraic expressions obtained from the spatial discretization of the governing equations. In the present research, differentiation is performed by rearranging the computer code in complex arithmetic form, and then the complex Taylor series expansion (CTSE) technique [13] is used to extract the derivative information. The CTSE technique yields a derivative error of the order of the machine accuracy. The step of the complex expansion can be as small as desired, because the formulas are not affected by cancellation error as in finite differences. In FORTRAN, the run time for complex arithmetic routines is approximately three–four times the run time of real arithmetic routines. Run-time considerations limit the number of sensitivity-information data points that can be included in the model.

III. Kinetics for HMX–HTPB Propellants: BDP Model

The following sets of equations are assumed to govern the species and temperature evolutions:

$$\begin{aligned} \rho c_p \frac{\mathrm{D}T}{\mathrm{D}t} &= \nabla\cdot(\lambda\nabla T) + \sum_{i=1}^{N_r} \alpha_i R_i, \\ \rho \frac{\mathrm{D}Y_k}{\mathrm{D}t} &= \frac{1}{Le_k}\nabla\cdot(\lambda\nabla Y_k) + \sum_{i=1}^{N_r} \beta_{i,k} R_i \end{aligned} \tag{2}$$

where $k = 1, \ldots, N_s$ and α_i and $\beta_{i,k}$ are coefficients based upon mass and total enthalpy conservation that are fully determined given a particular reaction scheme; one example is presented at the end of this section.

The most successful chemistry model to date for describing heterogeneous solid-propellant combustion using a small set of global reactions is the Beckstead et al. (BDP) [14] model, which postulates that reaction occurs along three preferred irreversible paths: a monopropellant decomposition flame, a primary diffusion flame, and a secondary diffusion flame.

The global chemistry reaction scheme is therefore described by a three-step mechanism. Step 1 is the HMX decomposition flame. Step 2 is the primary diffusion flame (HTPB vapor and HMX vapor). Step 3 is the secondary diffusion flame (HMX combustion products and HTPB vapor).

It is important to emphasize the concept of competitive paths. The decomposition flame and the primary diffusion flame compete for the HMX vapor. Therefore, the balance between the kinetic rate constants of the two steps dictates whether the conversion of gasification products to final product follows the combination path of step 1 plus step 3 or the direct path of step 2.

The BDP model is a phenomenological model based on global reaction paths; therefore, it does not specify the molecular composition of the species that take part in the three reaction steps. To assign values to the parameters of the reaction scheme, a set of assumptions about the chemical composition of the mixture is necessary. Experiments show that at low temperature, the gaseous products of the pyrolyzing binder comprise, in part, midweight molecular species (cyclic hydrocarbons consisting of multiple butadiene units) and, in part, light molecular species (specifically, ethylene, ethane, and propylene). It is not clear whether these monomer units are formed in the condensed-phase degradation or in the gas phase. It is postulated that the fraction of light species increases with temperature, and for gas temperatures relevant to a solid-propellant-rocket system, the solid binder decomposes into ethylene (C_2H_4).[§] Equilibrium-detailed chemistry computations led to the identification of the products of the decomposition of HMX as a mixture of CO, CO_2, N_2, H_2O, and H_2. The vapors of the HMX gasification are assumed to comprise a mixture of gaseous HMX ($C_4H_8N_8O_8$) and HMX decomposition products, with a mass ratio dictated by the heat release in the solid phase, which is assigned from experimental data. The final products of HMX–HTPB combustion are essentially CO, N_2, and H_2, according to equilibrium calculations. Note that for this simple scheme, the secondary diffusion flame represents an endothermic reaction and so is inappropriately identified as a flame in the classical sense. Here, the word flame is used as a region of large chemical activity, not necessarily associated with exothermic reactions.

According to these assumptions, the steps of the global scheme can be written as

HMX decomposition:

$$C_4H_8N_8O_8 \rightarrow 3CO + CO_2 + 3H_2O + H_2 + 4N_2$$

Primary diffusion flame:

$$C_4H_8N_8O_8 + 2C_2H_4 \rightarrow 8CO + 4N_2 + 8H_2$$

Secondary diffusion flame:

$$3CO + CO_2 + 3H_2O + H_2 + 4N_2 + 2C_2H_4 \rightarrow 8CO + 4N_2 + 8H_2$$

If the three active mixtures are denoted as Y_i (where $i = 1, \ldots, 3$) with $\mathrm{HMX_{vapor}} \rightarrow i = 1$, $\mathrm{HMX_{prod}} \rightarrow i = 2$, and $\mathrm{HTPB_{vapor}} \rightarrow i = 3$, the reaction rates associated with the three global steps are expressed in general form:

$$R_i = D_{g,i} P^{n_i} T^{m_i} \prod_{k=1,N_s} Y_k^{\nu_{i,k}} \exp\left(-\frac{\theta_i}{T}\right) \tag{3}$$

Note that the expressions are made as general as possible so that the performance of the optimization scheme can be tested. For global

[§]Private communications with R. Yetter, January 2005.

kinetics, the species exponents $\nu_{i,k}$ in the reaction rates do not need to be related to the stoichiometric coefficients of the corresponding reaction; their values should be assigned via the optimization strategy.

A. Surface Gasification and Heat Release

Chemical decomposition in the solid/molten phase is not modeled. A set of pyrolysis laws, one for each solid-phase ingredient, is assumed to govern the gasification. For heating rates typical of the deflagration wave in most solid propellants, it was demonstrated that a linear pyrolysis law is consistent with the physics underlying a single-step decomposition in the solid phase [15] and matches experimental data with satisfactory accuracy [16]. A pressure-power-law dependence can also be considered and so we define

$$r_{b,\mathrm{hmx}} = D_{s,\mathrm{hmx}} P^{\mu_{\mathrm{hmx}}} \exp(-\Theta_{\mathrm{hmx}}/T_s) \tag{4a}$$

$$r_{b,\mathrm{htpb}} = D_{s,\mathrm{htpb}} P^{\mu_{\mathrm{htpb}}} \exp(-\Theta_{\mathrm{htpb}}/T_s) \tag{4b}$$

The accuracy of a pyrolysis law in describing surface gasification is diminished by the observation that linear pyrolysis parameters, when determined from bulk heating experiments, depend upon the propellant heating rate. Such parameters are usually measured with heating rates that are several orders of magnitude smaller than those that are characteristic of the propellant thermal wave [17]. For the same reason, there is no guarantee that pyrolysis laws determined in such a way are an accurate approximation for conditions other than the one-dimensional steady state, even though an activation-energy asymptotic analysis would suggest otherwise. The issue is that the previous statement requires the decomposition kinetics to be independent of the thermal wave. The same argument applies to modifications such as those proposed by Brewster [6], which take into account the surface-temperature gradient in the solid phase when defining pyrolysis laws for unsteady regressions.

Chemical reactions in the solid phase are lumped at the surface, thus the heat release corresponds to the heat of sublimation of the solid material. In our model, the specific heats of the solid and gas phases are assumed equal, and so the heat release equals the ratio between the heat flux balance at the surface and the mass flux; hence, the thermal boundary conditions are

$$[\lambda \boldsymbol{n} \cdot \nabla T] = -Q_s \dot{m}, \qquad [T] = 0 \tag{5}$$

where the jump operator $[\cdot]$ subtracts the solid value from the gas value. For HTPB, the heat release in the solid phase is determined by an energetic balance in the gasification layer. Assuming that the gasification product is C_2H_4 and that the heat of formation of HTPB is ≈ -7 cal/g, a value of $Q_{s,\mathrm{htpb}} \approx -455$ cal/g is obtained (a negative heat of sublimation is indicative of an endothermic reaction). This value is in line with the measurements of Esker and Brewster [17] (-460 cal/g) and those of Cohen et al. [18] (-430 cal/g).

The reaction paths of solid HMX as it passes through the thermal wave are not well established. Detailed models by Davidson and Beckstead [19] and Prasad et al. [20] revealed that at high pressure, evaporation is predominant over chemical decomposition, an outcome that implies that the heat release at the surface decreases with an increase in pressure. However, experimental investigations by Zenin [21] and Lengelle [22] contradicted these findings, showing that the heat release in the solid phase is an increasing function of the pressure for a steadily burning propellant. According to the experiments, for the range of pressure of interest in our multidimensional simulations ($P = 40$–100 atm), a constant value of $Q_{s,\mathrm{hmx}} = +100$ cal/gm is used. The values for variables related to the gasification equations are listed in Table 1.

The coefficients α and β in Eq. (2) are obtained based upon enthalpy and mass conservation:

$$\alpha = \begin{bmatrix} 794.2 & 3000 & -1169.6 \end{bmatrix} \text{cal/g}$$

Table 1 Relevant parameters of the gasification of each HMX and HTPB ingredient

$D_{s,\mathrm{hmx}}$	1.8×10^6 cm/s
Θ_{hmx}	1.27×10^4 K
$D_{s,\mathrm{htpb}}$	3.82×10^3 cm/s
Θ_{htpb}	1.22×10^4 K
$Q_{s,\mathrm{hmx}}$	100 cal/gm
$Q_{s,\mathrm{htpb}}$	-455 cal/gm
μ_{hmx}	0
μ_{htpb}	0

$$\beta = \begin{bmatrix} -1 & -5.25 & 0 \\ 1 & 0 & -5.25 \\ 0 & -1 & -1 \end{bmatrix}$$

B. Transport and Inertial Coefficients

The thermal conductivity in the solid phase is taken to be constant for each ingredient (fuel matrix and oxidizer), whereas in the gas phase, it is assumed to vary according to the temperature power law $\lambda_g = a_\lambda (T/T_{\mathrm{ref}})^{e_\lambda} + b_\lambda$. As a first-order approximation, the power law is assumed to be valid independently of the gas composition. The specific heats in the gas and solid phases are constant. The transport coefficients are listed in Table 2.

C. Gas-Phase Kinetics Calibration

The gas-phase kinetic reaction parameters are determined exclusively as a part of the optimization procedure and are listed next [cf. Eq. (3)]:

1) The preexponential reaction terms are $D_{g,1\text{–}3}$.
2) The activation temperatures are $\theta_{1\text{–}3}$.
3) The reaction-term pressure exponents are $n_{1\text{–}3}$.
4) The reaction-term temperature exponents are $m_{1\text{–}3}$.
5) The reaction terms are $\nu_{1,1}$, $\nu_{2,1}$, $\nu_{2,3}$, $\nu_{3,2}$, and $\nu_{3,3}$.

The species exponents not reported in the last line of the preceding list are set to zero, because the species to which they refer do not take part in the corresponding reaction.

Because HMX self-deflagrates, it can be calibrated a priori (i.e., without knowledge of the diffusion flames). As mentioned in the preceding section, only parameters of the gas-phase reaction scheme are optimized. The choice of the burn characteristics is fundamental. A sensible choice would include steady burn-rate data at different pressures, supply-temperature sensitivity, and T-burner pressure-response data. The supply-temperature sensitivity is defined as $\sigma = (\partial r_b/\partial T_0)/r_b$, where r_b is the steady-state burning rate and T_0 is the cold supply temperature. In the regime of vanishingly small pressure fluctuations, the pressure-response curve can be related to the pressure exponent n_p, the pyrolysis parameters, and the cold-temperature sensitivity using the Zel'dovich–Novozhilov theory [23]; that is,

$$A = (T_s - T_0)\frac{\Theta_{\mathrm{solid}}}{T_s^2} \tag{6a}$$

Table 2 Relevant transport parameters for both the gas and solid phases

$\lambda_{s,\mathrm{hmx}}$	6.3×10^{-4} cal/cm · s · K
$\lambda_{s,\mathrm{htpb}}$	4×10^{-4} cal/cm · s · K
a_λ	1.25×10^{-4} cal/cm · s · K
e_λ	0.7
b_λ	0
T_{ref}	700 K
$c_{p,\mathrm{gas}}$	0.3 cal/gm · K
$c_{p,\mathrm{solid}}$	0.3 cal/gm · K

$$B = \frac{1}{(T_s - T_0)\sigma} \tag{6b}$$

$$\alpha_s = \left(\frac{\lambda_s}{\rho_s c_p}\right)_{\text{solid}} \tag{6c}$$

$$\Lambda = \tfrac{1}{2}[1 + \sqrt{1 + (8i\pi f \alpha_s / r_b^2)}] \tag{6d}$$

$$R_p = \frac{n_p AB}{\Lambda + (A/\Lambda) + AB - (1 + A)} \tag{6e}$$

where the subscript solid refers to either the HMX or the HMX–HTPB blend. In the latter case, the blend properties are evaluated using the homogenization formulas detailed by Chen et al. [24]. At the pressures under consideration, the finest HMX particles (4 μm) are smaller than the HMX melt layer for a 1-D thermal wave: Zenin [21] measured a melt-layer thickness of 15 μm at 70 atm. Homogenization models based on properties and size distribution in the solid state are still assumed to be valid, because of the little difference between solid and liquid thermal characteristics and the short particle residence time in the melt layer that does not allow for a complete mixing.

Though the values for r_b, σ, and R_p data are not independent, a collection of burning characteristics comprising only steady burn rates and supply-temperature sensitivities does not convey information about the thermal length scale of the solid-phase heat conduction (in this case, α_s / r_b). The steady burn rate is, in fact, independent of the solid-phase thermal conductivity. The use of T-burner data fills this void because of the dependency of Λ on the thermal length scale.

1. *Pure-HMX Data*

The steady burn-rate data are taken from Lengelle [16], who also reported measurements performed by Boggs. The sensitivity data of Beckstead et al. [25] are used, and the T-burner pressure-response data of Finlinson et al. [26] (also reported by Brewster [6]) are also considered.

The success of the optimization approach depends critically on the quality of the burning characteristics used in the calibration step. When comparing the calibration data with other documented measurements, the burn-rate percent error evaluated using the data of Lengelle [22], Zenin , and Atwood et al. [27] is roughly in the range of 0–50%; specifically, at 70 atm, roughly the median value of the pressure range investigated in this analysis, the percentage of relative error is above 30%. The sensitivity data are very scattered, with a maximum error higher than 30% when we compare Zenin's data [28] with the measurements reported by Beckstead et al. [25]. The Finlinson et al. [26] T-burner pressure-response data are the only data we found in the open literature and no error bars are given.

2. *HMX–HTPB Pseudopropellant Data*

Propellant-blend burning characteristics taken from Beckstead and McCarty [3] are used to calibrate the heterogeneous reactions: namely, reactions R_2 and R_3. Only steady burn-rate measurements are available; no other source of experimental data is used to verify the accuracy of the data. The calibration points correspond to two propellant formulations with only monomodal distributed HMX particles of 4-μ nominal diameter and solids fractions of 70 and 78%. This size of particle is assumed to be small enough to support premixed combustion; at the same time, the morphological scales are deemed to be much smaller than the solid thermal scale, and so the samples support a one-dimensional thermal field. This conclusion is assumed to be true for all of the pressures considered, and it is emphasized that in the 1-D calibration procedure, the heterogeneous reactions R_2 and R_3 are still denoted as diffusion-flame reactions, despite the premixed nature of the streams.

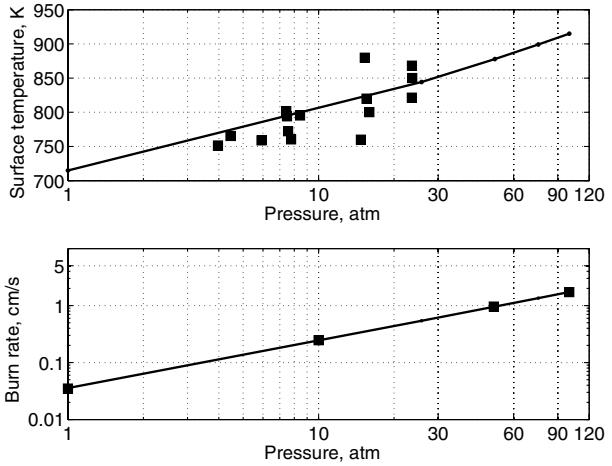

Fig. 1 Optimal results for the calibration of pure HMX in model 1; model prediction (solid line) and experimental (target) measurements (symbols).

IV. Optimized Models

The investigation focuses on three models differing in regard to both the parameter space and the burning characteristics that form the objective function [Eq. (1)]. The goal of the analysis is to determine the efficacy of the optimization technique by building models of increasing complexity. The three models detailed in this section were also reported in a concise form by Massa et al. [7]. In that publication, the emphasis was on the optimization procedure itself, whereas our investigation focuses on the relation between the 1-D-based optimization and multidimensional computational analysis.

A. Model 1

In the first model considered, optimization is carried out on a subset of the model parameters. The species exponents $\nu_{i,k}$ are set to unity, and the temperature exponents m_i are set to zero. The rationale for these two choices is the desire to keep the kinetic rate expressions in line with previous modeling attempts [9–11]. The burning characteristics include pure-HMX steady burn rates in the pressure range of 1–100 atm; pure-HMX burn-rate sensitivity at $T_0 = 300$ K and $P = 20$ atm; and pseudopropellant burn-rate data for pressures of 40, 68, and 108 atm and solid loadings of 70 and 78%. A comparison between experiments and model predictions is shown in Figs. 1–3. Figures 1 and 2 refer to pure HMX, whereas Fig. 3 shows the comparison between experiments and predictions for pseudopropellant deflagration. Burn rates for all of the measurements [3] (solid compositions, sizes, and pressures) are also shown. The optimized gas-phase kinetics parameters are listed in Table 3.

A critical analysis of the parameters in Table 3 shows that the secondary diffusion flame is very strong compared with both the primary and decomposition flames. The secondary diffusion flame corresponds to an endothermic reaction in which the ethylene strips an oxygen atom from each molecule of carbon dioxide and water. Yetter[¶] argues that such a reaction is likely to be very slow and play a minor role in determining the burn rate. As will be evident from the following analysis, it is not possible to obtain good agreement with the pseudopropellant experiments of Beckstead and McCarty [3] if the secondary diffusion flame is completely discarded.

A key perspective in the physical interpretation of the parameters of model 1 is obtained by recognizing that in the limit $D_{g,3} \to \infty$, the conversion of gasification products to final products along the path of step 1 plus step 3 is controlled by the decomposition flame, the slowest reaction. The overall result is equivalent to a reaction with

[¶]Private communications with R. Yetter, January 2005.

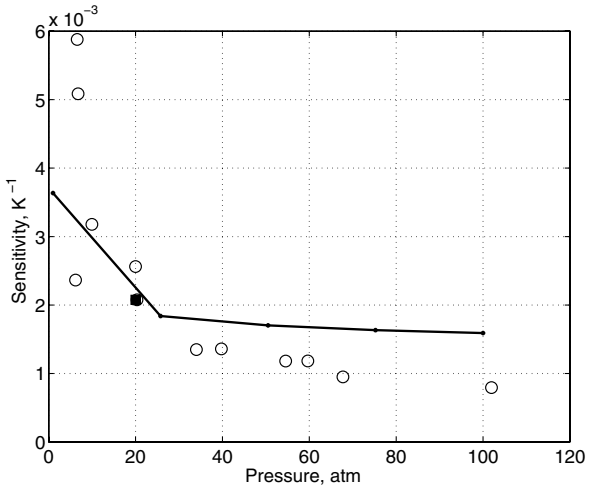

Fig. 2 Optimal results for the calibration of pure HMX in model 1; cold-temperature burn-rate sensitivity; data points used in the calibration (filled symbols); remaining data points (open symbols) are reported but not used.

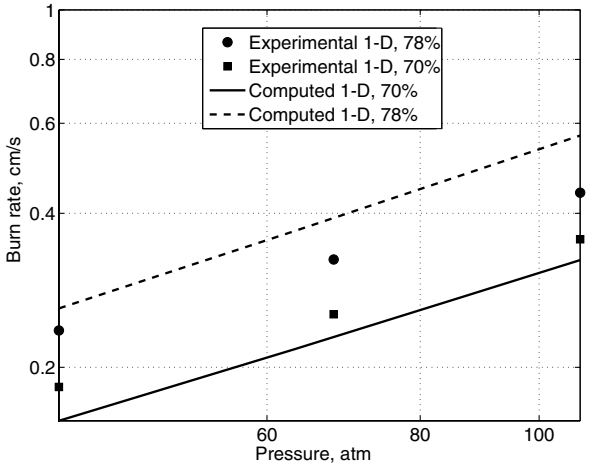

Fig. 3 Comparison of optimal results and experiments for model 1; predicted burn rates for two solid loadings (lines) and measurements (symbols) [3]; all experimental data points are used as targets in the calibration.

kinetics governed by the HMX decomposition rate constant, but with a cooler flame temperature. The associated adiabatic flame temperature depends only on the solid loading and is identical to the flame temperature of the primary diffusion-flame path (step 2). Although both the combination path of step 1 plus step 3 and step 2 lead to a lower flame temperature, the combination of the HMX flame plus an infinitely strong secondary flame is fundamentally different from the direct path along the primary diffusion reaction. The rationale is that the primary diffusion and the decomposition flames are competitive phenomena, and so for the reactants to burn within step 2, the primary diffusion flame must be stronger than the decomposition flame that is fixed by the pure-HMX calibration. In this scenario, a primary diffusion flame much stronger than the monopropellant flame would lead to an increase in the burn rate, because the flame is pushed closer to the propellant surface, even though the flame temperature is lower than that of the pure-HMX flame. These considerations lead to the conclusion that in the context of model 1, a strong endothermic secondary flame is necessary to explain the burn-rate reduction associated with the presence of the HMX.

Table 3 Relevant parameters to the HMX–HTPB deflagration for model 1

$D_{g,1}$	2.869 gm/(cm^3 · s atm^{n_1})
θ_1	1.8×10^3 K
n_1	1.787
$D_{g,2}$	4.4×10^1 gm/(cm^3 · s atm^{n_2})
θ_2	0
n_2	0
$D_{g,3}$	4.9×10^3 gm/(cm^3 · s atm^{n_3})
θ_3	1.63×10^2 K
n_3	2.9

B. Model 2

The second model uses a larger set of design parameters and a larger set of burning characteristics to define the objective function. The species-mass-fraction exponents $\nu_{i,k}$, along with the temperature m_i, are considered for all of the reactions $i = 1, 2, 3$ and all of the species $k = 1, 2, 3$. The secondary diffusion flame is dropped by setting $D_{g,3} = 0$, and so this model provides insight into the contribution of the primary flame to the propellant deflagration. Pure-HMX burning characteristics include steady burn-rate data in the pressure range of 1–100 atm, sensitivity at $T_0 = 300$ K and $P = 20$–40 atm, and T-burner pressure-response data [26].

We use only two sensitivity σ data points, even though experimental measurements for a larger set of pressures are available, for two reasons. First, the increased run time required to evaluate sensitivity information limits the number of observations to be included in the model (cf. Sec. II.B). Second, information about the cold-temperature sensitivity is contained in the T-burner pressure-response data [cf. Eq. (6b)], measured at pressures of 14 and 68 atm.

For pseudopropellants, the set of burning characteristics is augmented by requiring that the deflagration intrinsic stability condition is satisfied for all pressures and solid loadings considered in the calibration. The stability condition is evaluated by computing the temporal growth rate of small perturbations to the steady condition identified by the surface temperature T_s and the burn rate r_b. Letting $\zeta = \theta_{\text{blend}}(T_s - T_0)/RT_s^2$ for $\zeta > 1$, the stability condition is equivalent to

$$\tfrac{1}{2} - \sqrt{\tfrac{1}{4} + 2\zeta} < G' < \tfrac{1}{2} + \sqrt{\tfrac{1}{4} + 2\zeta} \tag{7}$$

where

$$G' = L_s \frac{\mathrm{d}g}{\mathrm{d}T_s}, \qquad L_s = \frac{\lambda_s}{\rho_s r_b c_p} \tag{8}$$

and $g(T_s)$ is the normal component of the temperature gradient at the solid side of the burning interface. Note that instability occurs both for negative and positive values of G'. The former case occurs at low pressures and low solid loadings. This condition plays a role in establishing low-pressure and low-loading deflagration limits originating from stability considerations. Comparison between experiments and predictions are summarized in Figs. 4–7. The

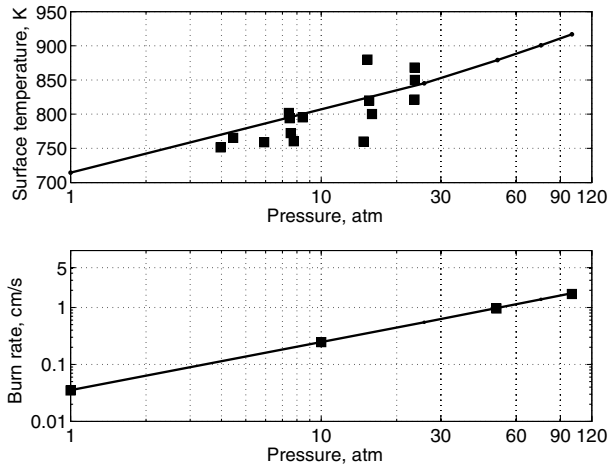

Fig. 4 Optimal results for the calibration of pure HMX in model 2.

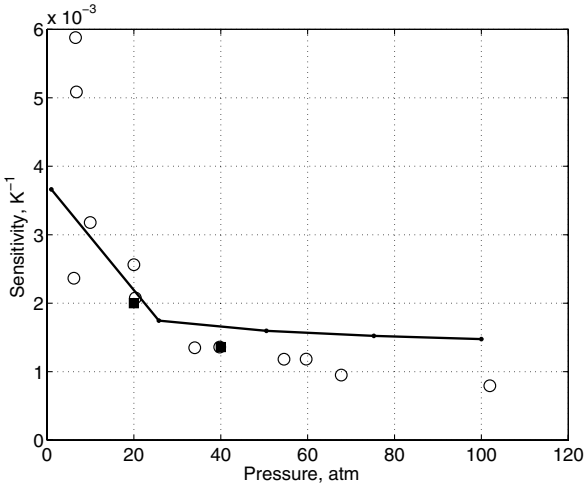

Fig. 5 Optimal results for the calibration of pure HMX in model 2, cold-temperature burn-rate sensitivity; data points used in the calibration (filled symbols); remaining data points (open symbols) are reported but not used.

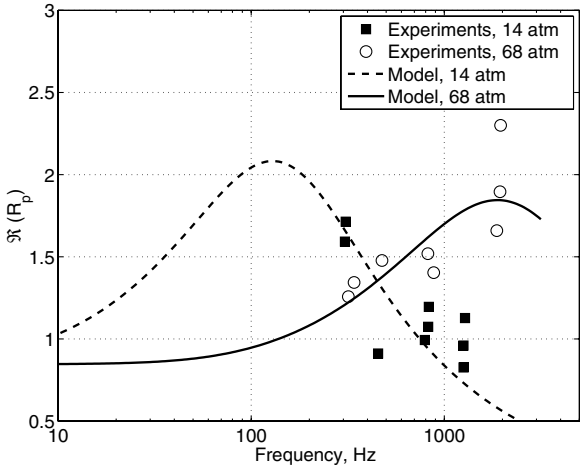

Fig. 6 Optimal results for the calibration of pure HMX in model 2; comparison with T-burner pressure-response data (symbols); all experimental data points are used as targets in the model calibration.

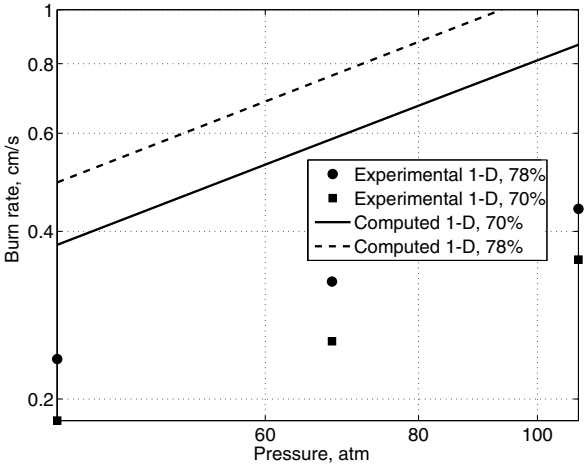

Fig. 7 Comparison of optimal results and experiments for model 2; burn rates for pseudopropellants of different solid loadings compared with experiments (symbols) [3]; all experimental data points are used as targets in the model calibration.

Table 4 Relevant parameters to the HMX–HTPB deflagration for model 2[a]

$D_{g,1}$	5.6×10^3 gm/(cm^3 · s atm^{n_1})
θ_1	2.5×10^3 K
n_1	1.8
m_1	−1
$\nu_{1,1}$	0.5
$D_{g,2}$	2.75×10^1 gm/(cm^3 · s atm^{n_2})
θ_2	9.84×10^3 K
n_2	0.8
m_2	1.48
$\nu_{2,1}$	0.51
$\nu_{2,3}$	3.74

[a]The parameters of the secondary diffusion flame are not listed because the secondary flame was not considered in this model.

optimal parameters for model 2 are listed in Table 4. Noting that the results reported in Fig. 7 are optimal given the parameters and performance selected, we conclude that model 2 predicts blend burn rates with considerably larger errors than those of model 1 (cf. Fig. 3) and that this outcome is linked to the absence of a secondary flame.

C. Model 3

The observation that led to the development of a third kinetic model is that the three-step scheme presented in Sec. III is not able to explain the burn-rate diminution due to the presence of binder shown in the experiments, unless a nonphysical strong secondary flame is assumed. To circumvent this difficulty while remaining in the framework of an irreversible three-step scheme, the assumption is made that the presence of the binder can inhibit the pure-HMX kinetics and produce an overall anticatalytic effect on the HMX reaction rate. To model this, the HMX-flame reaction-rate expression in Eq. (3) is transformed by

$$R_1 \rightarrow R_1 \times (1 - Y_3)^{\nu_{1,3}} \tag{9}$$

where Y_3 is the mass fraction of the ethylene in the mixture. The addition of the new parameter $\nu_{1,3}$ allows us to improve the optimal calibration within the same systematic framework. Note that in a global kinetic model, the form of the reaction-rate terms dependent on species concentration is not directly derived from stoichiometry considerations as it would be for a detailed mechanism. Therefore, the addition of a term dependent on the mass fraction of ethylene in the HMX rate expression is not in contradiction with the kinetic model itself; it is an extension of the argument by which noninteger species exponents are used for the species concentrations in model 2. Moreover, the transformation of Eq. (9) allows for the HMX kinetics to be calibrated independently of the diffusion-flame calibration, as in the previous two models. Therefore, results for pure HMX will not be shown in this section, being identical to those presented for model 2.

The same set of burning characteristics used for the calibration of model 2 is considered. Comparison between experiments and model predictions, for the pseudopropellant only, are summarized in Fig. 8. It should be noted that the calibration error is significantly smaller than that of models 1 and 2.

The optimal parameters for model 3 are listed in Table 5. The limited number of burning characteristics for blends and, in particular, the absence of measurements of sensitivity information prevent us from obtaining a meaningful calibration for every parameter. In fact, some parameters have a small effect on the objective function, and so function values not significantly different may correspond to considerably different values of these parameters. For example, in Table 5, the species-mass-fraction exponents $\nu_{3,2}$ and $\nu_{2,3}$ have values of around 20. These two parameters have little influence on the particular objective function. Large values of the species exponents can be limited by imposing proper bounds on the calibration parameter space.

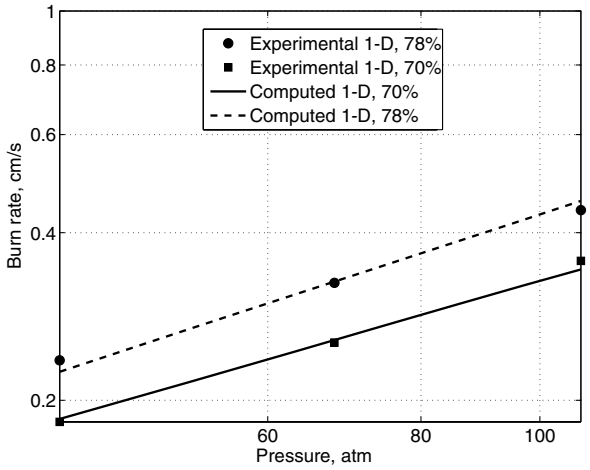

Fig. 8 Comparison of optimal results and experiments for model 3; the format is identical to that of Fig. 7.

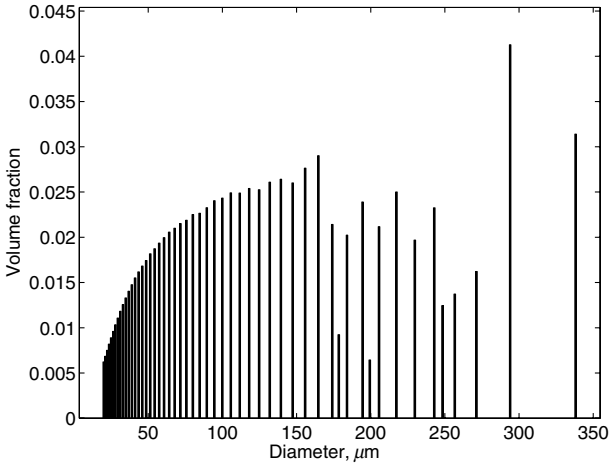

Fig. 9 Volume distribution among the particle diameters.

V. Multidimensional Analysis

The fundamental issue in the development of simplified kinetics models for solid propellant lies in the accuracy of reaction formalisms calibrated against 1-D burning characteristics when applied to deflagration supported by a three-dimensional, intrinsically random, combustion field. This issue has not received enough attention in past literature, particularly when it is noted that most solid propellants used in aerospace applications have oxidizer particles larger than the thermal length scale. The goal of the set of computations presented in this section is to quantify the ability of models that are 1-D-optimal to predict the burning characteristics of 3-D propellants (particularly, propellants characterized by having particles larger than, or comparable in magnitude to, the thermal scales in the solid phase, nonnegligible surface corrugation, and gas-phase chemistry with noticeable diffusion effects).

A. Packs

The first pack chosen to conduct a multidimensional analysis contains an HMX bimodal size distribution identified as mix A: 42.75% at 200 μm and 42.75% at 58 μm. A bar plot of the volume fraction and a vertical slice plot displaying particle location are shown in Figs. 9 and 10; note that the convention used in this and the following figures is to use the x and z Cartesian coordinates to represent the plane normal to the average regression speed and to use y to indicate the height above the plane. A log-normal distribution is independently assumed for each cut. In Fig. 9, the irregularities in the distribution for large diameters are due to the diameter consolidation necessary when dealing with integer numbers of particles [29]. The total number of particles is 1×10^4, the largest sphere has a diameter of 338 μm, and the smallest sphere has a diameter of 20 μm. The

Table 5 Parameters relevant to the HMX–HTPB gas-phase chemistry for model 3[a]

$\nu_{1,3}$	8.9
$D_{g,2}$	1.34×10^4 gm/(cm$^3 \cdot$ s atm^{n_2})
θ_2	2.62×10^2 K
n_2	0.03
m_2	3.8
$\nu_{2,1}$	5.0
$\nu_{2,3}$	17.9
$D_{g,3}$	1.87×10^2 gm/(cm$^3 \cdot$ s atm^{n_3})
θ_3	7.14×10^3 K
n_3	0.005
m_3	3.54
$\nu_{3,2}$	20.0
$\nu_{3,3}$	8.27

[a]The parameters of the HMX flame (with the exception of $\nu_{1,3}$) are identical to those tabulated in Table 2, and are therefore not listed.

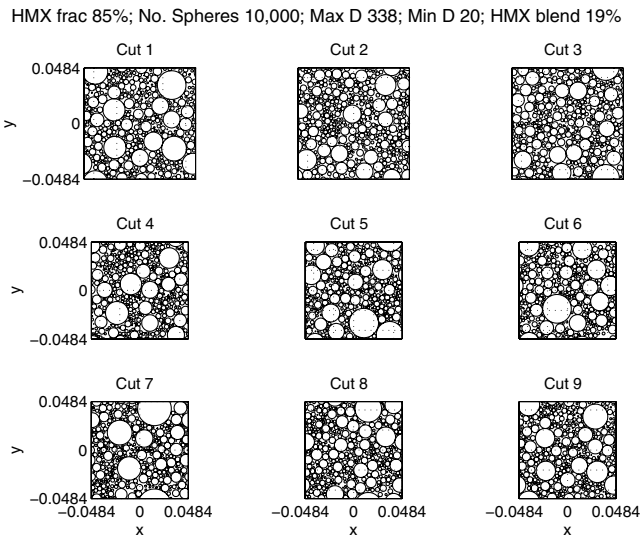

Fig. 10 Slices of the computational representation of the multidimensional propellant for pack A, identified by the mass-fraction/cut-diameter combinations of 42.75% at 200 μm and 42.75% at 58 μm; lengths are expressed in centimeters.

first pack is referred to in the following as pack A. Note that in this paper, we explicitly differentiate between the experimental specification of the propellant (mix) and its computational representation as spheres randomly packed in a periodic Cartesian domain (pack).

The second pack (pack B) has a bimodal distribution of particles, with cuts specified by the following mass-fraction/nominal-diameter set (mix B): 42.75% at 200 μm and 42.75% at 4 μm. In pack B, all of the 4-μm cut is homogenized with the binder. A slice plot of the second pack is shown in Fig. 11; note that the overall solid loading is identical to that of the previous pack, but a large volume fraction of the matrix region is occupied by oxidizer. This region is treated in the computations as a homogeneous propellant blend (a fine mix of HMX and HTPB). The thermal and inertial properties of the blend are evaluated by using rationally derived homogenization formulas, as detailed by Chen et al. [24].

Both packs are cubic periodic packs, in which periodic boundary conditions are imposed at the faces parallel to the mean burning direction. The side of the cube has the dimensions of 970 μm for the first pack and 475 μm for the second. More details about the algorithms used to generate the packs can be found in Knott et al. [30] and Kochevets et al. [29].

B. Numerical Method

We solve the 3-D field equations using the Oseen approximation to determine the fluid-dynamics fields. The Oseen approximation

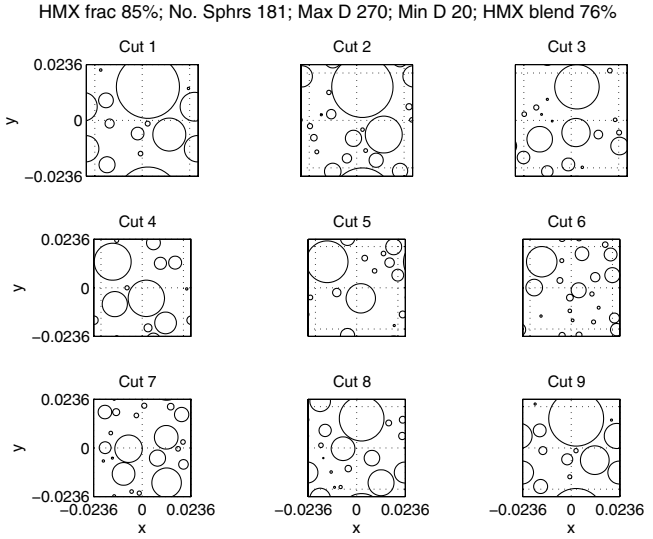

Fig. 11 Vertical slices through pack B with a bimodal distribution of oxidizer (42.75% at 200 μm and 42.75% at 4 μm); all of the fine cut is homogenized in the matrix.

assumes that the stream tubes can be regarded as vertical structures of a constant cross-sectional area. When applied to a multidimensional deflagrating propellant with a corrugated surface, the mass flux within each stream tube is found by accounting for the total volume of propellant swept by the regressing front. A 3-D computational analysis presented in Massa et al. [31] demonstrates that the relative computed burn-rate error between Oseen and Navier–Stokes predictions is less than 10%, well within the measurement error bars (cf. Sec. III.C.1). More detail on the application of such an approximation to propellant deflagration analysis can be found in Jackson and Buckmaster [2]. The nonlinear PDE set is discretized using the Crank–Nicholson scheme; the resulting linear system is inverted with a Newton–Krylov (GMRES) solver. More details of the solution algorithm can be found in Massa et al. [32].

The computational simulations are performed on a distributed-memory Apple G5 cluster located at the University of Illinois. The computational meshes have the size of $[152 \times 152 \times 52 \times 2]$: the first two numbers indicate the mesh dimensions in the plane normal to the average burning direction, the third number indicates the number of mesh points in the burning direction, and the last number indicates that meshes of identical dimensions are used in the solid and gas phases. The simulations require approximately 1 h per 3 ms of burning on 64 processors.

C. Domain Dimension Analysis

Periodic randomly packed propellant samples accurately represent a deflagration under zero crossflow conditions provided that the dimensions of the domain are large enough to not introduce an artificial nonphysical length scale. The relation between the domain size and the surface-averaged burn rate is explored in the context of AP–HTPB propellant by Massa et al. [33]. The domain size influences the deflagration process for HMX–HTPB propellant more profoundly than for AP–HTPB propellant because of the large difference between the deflagration characteristics of the two solid ingredients. Moreover, the irregular burning behavior is expected to be accentuated when the percentage of coarse oxidizer cut is increased. Consequently, it is appropriate to restrict the analysis to pack A.

This section presents an analysis of the effect of the domain size on the burn rate by considering a pack of identical oxidizer composition as pack A (cf. Sec. V.A), but with a substantially larger domain (1610 vs 970 μm for the edge of the x–z section) and a larger number of particles (20,000 vs 10,000). The pack denoted as pack C has a rectangular x–y section, with a height of 700 μm. The validation is carried out at a single pressure of 68 atm because of the large computational resources required to simulate large packs. The computed average regression rate for pack A is equal to 0.335 cm/s, whereas for pack C, it is equal to 0.286 cm/s, with a relative error approximately equal to 15%. The experimentally measured average regression rate is 0.323 cm/s. The difference between the two computational results is considered comparable to measurement errors and therefore acceptable, based on the magnitude of the measurement error for pure HMX discussed in Sec. III.C.1 and comments about the reliability of the experimental data for HMX–HTPB mixes reported by Beckstead and McCarty [3]. Therefore, results are presented in the next section using pack A.

VI. Multidimensional Results

The experimental data of Beckstead and McCarty [3] are summarized in Fig. 12, in which the burn rate of each mix is plotted against the burn rate averaged over all mixes with equal solid loading; results for loadings of 70 and 78% are separated in the two panels. The filled symbols are reserved for the propellant blends, and the dashed lines represent ±40% deviations from the average. The measurements show only a slight effect of the particle size on the time–space-integrated regression speed. The overall trend shown by the experiments is that the particle size effect on the burn rate is stronger at high pressure. Nonetheless, 3-D burning effects are observed to be pronounced, as demonstrated by the highly corrugated burned sample surface. These two observations are in contrast with the experimental evidence relating deflagration characteristics to the particle size in AP-based propellants, and they suggest that in HMX-based propellants a fundamentally different oxidizer–fuel interaction is present. Even though the pack morphology has a scarce influence on the regression rate, the role of diffusion flames cannot be dismissed as insignificant, based upon the sharp reduction in the burn rate with a decrease in solid loading observed in propellant blends: the burn-rate reduction cannot be explained by assuming an inert oxidizer–fuel interaction, as demonstrated in Sec. IV.

A. Model 1

No burn-through time result was obtained using model 1; quenching of the specimen was obtained for both packs at all pressures. This outcome is associated with the nonphysical fast secondary flame detailed in the model description section. The burning history for pack A at 68 atm is shown as a paneled series of temperature color maps in Fig. 13. In this figure, it should be noted that the HMX particles ignite immediately when exposed to the hot gases, but not enough heat is generated to sustain the pyrolysis of the endothermic binder. According to experimental observations by Beckstead and McCarty [3], HMX–HTPB propellant burns very irregularly; the term *intermittent burning* is used to describe the deflagration process. Two factors are primarily responsible for deflagration irregularity in heterogeneous mixes. The first is the large difference in regression speed of the two solid ingredients for typical

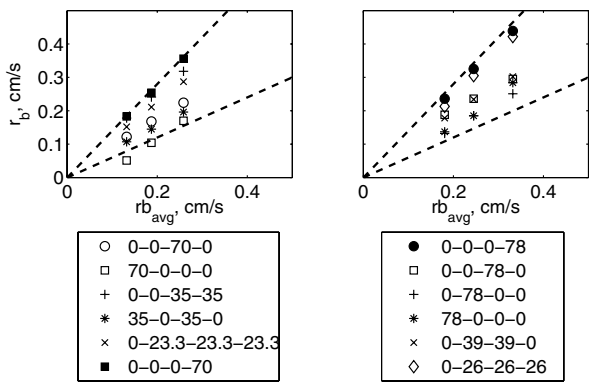

Fig. 12 Experimental data taken from Beckstead and McCarty [3]; ±40% deviations from the average (dashed lines); the four numbers in each legend item detail the percentage of the four reported cuts: 400, 200, 58, and 4 μm.

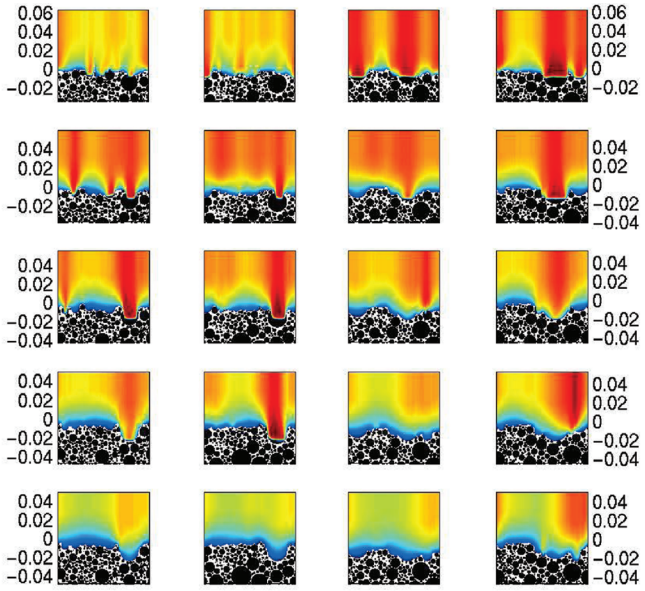

Fig. 13 Numerical experiment in which quenching of the sample occurs for model 1 and pack A; temperature color map with a scale range of 700 (blue) to 3300 (red); panels span in the horizontal direction across the pack and in the vertical direction in time; space lag between adjacent columns is 242 μm and time-lag between adjacent rows is 5×10^{-3} s.

deflagration values of the surface temperature: HMX is considerably faster than HTPB. The second is the energetic disparity of the surface gasification reactions: the binder is strongly endothermic, whereas the oxidizer is exothermic. The disparity in burning behavior at the surface leads to quenching of heterogeneous propellant if the pyrolysis of the binder is not adequately supported by the gas-phase thermal feedback. The conclusion is that even though model 1 produces pure-HMX and homogeneous-blend burning characteristics in good agreement with experiments, the kinetic model is not adequately calibrated to yield accurate predictions for heterogeneous propellants.

B. Models 2 and 3

Burn-rate predictions for model 2 and 3 are shown in Figs. 14 and 15 for pack A and pack B, respectively. Complete burning of the packs is achieved. This outcome confirms the conjecture that the quenching obtained with model 1 is due to a secondary diffusion flame of nonphysical strength.

Models 2 and 3 are characterized by having the same monopropellant flame model, but encompassing a different

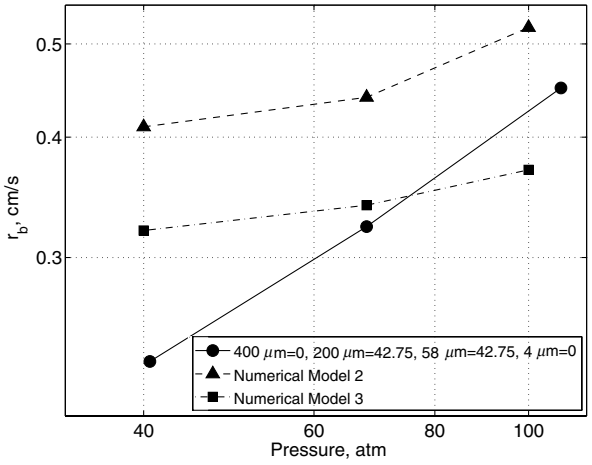

Fig. 14 Comparison between predicted burn rates and experiments [3] for pack A; size of the HMX particles follows a bimodal distribution with 42.75% at 200 μm and 42.75% at 58 μm.

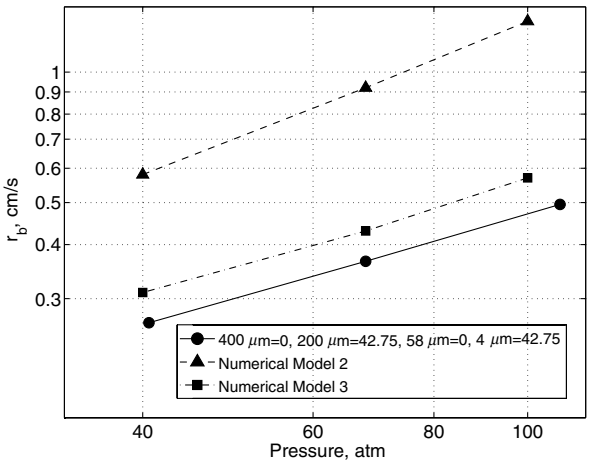

Fig. 15 Comparison between predicted burn rates and experiments [3] for pack B; size of the HMX particles follows a bimodal distribution with 42.75% at 200 μm and 42.75% at 4 μm.

treatment of the diffusion flames. The computational analysis shows that for both packs and for all pressures, model 3 yields burn rates significantly closer to the experiments than those of model 2, indicating a better treatment of the heterogeneous reactions. The diminishing of the error with the increase in the complexity of the model demonstrates the validity of the optimization approach: the better 1-D calibration yields the better model.

Experiments and model 3 computations also agree on a series of qualitative observations. The sensitivity of the computed burn rates to the particle size increases with pressure; moreover, the pressure exponent is lowered when the particle size is increased. In the computations, however, the pressure exponent is significantly more sensitive to the particle size than in the experiments. As a result, the pressure exponent is accurately matched for pack B, whereas it is markedly underpredicted for pack A. The deviation between predictions and measurements is quantified by calculating the percent ratio between the error L2 norm (integrated over the pressure range) and the mean measured burn rate (integrated over the pressure range) for both packs and models. For model 2, this ratio is 39 and 117% for pack A and pack B, respectively. For model 3, the same ratio is reduced to 19 and 20%. Note than an error of 20% is well within the range of typical measurement error for the solid-propellant burn rate. Consider as a reference the errors reported in Sec. III.C.1, in which the pure-HMX measurements are introduced.

Experimental data are often presented in terms of the burning-power-law coefficients A_p and n_p for the data best fit $r_b = A_p p^{n_p}$. For narrow and uncentered pressure ranges, it is convenient to center and rescale the pressure data (Massa et al. [7])

$$r_b = A_{\mathrm{pl}}(p/p^*)^{n_{\mathrm{pl}}/n^*} \tag{10}$$

to avoid cancellation of errors in the best-fit calculation of A_p and n_p. Suitable values for n^* and p^* are the standard deviation of $\ell_n\, p$ and the geometric mean pressure, respectively. A comparison between power-law coefficients calculated based on experimental data and predictions is reported in Table 6, which shows that model 3 produces satisfactory results for all of the parameters but the pressure exponent for mix A. Table 6 also shows that model 3 is significantly more accurate than model 2.

Table 6 Empirical analysis of the burn rates [cf. Eq. (10)]

	Experiments		Model 2		Model 3	
Mix[a]	A_{pl}, cm/s	n_{pl}	A_{pl}, cm/s	n_{pl}	A_{pl}, cm/s	n_{pl}
Mix A	0.33	0.36	0.45	0.11	0.34	0.071
Mix B	0.36	0.31	0.89	0.41	0.42	0.30

[a]The propellant mixes are defined in Sec. V.A.

Three-dimensional effects in HMX–HTPB deflagration are showcased in the next set of figures, which corresponds to model 3. Figure 16 shows the location of the burning surface at equal time intervals for pack A at 68 atm for a two-dimensional vertical cut. A three-dimensional view of the burning surface is presented for two representative times in Fig. 17, in which the surface temperature is shown as a color map, and the pack morphology is shown in the solid phase for two vertical cuts corresponding to the minimum x and z. A large degree of surface corrugation can be noted. The surface corrugation is an important parameter in determining the magnitude of multidimensional deflagration effects due to 3-D heat flow in the solid-phase thermal layer. Massa et al. [33] reduced the 3-D heat-conduction equation in the solid phase to a 1-D form by adding a series of source terms to obtain a predictive formalism, isolated the source term derived from the surface corrugation, and demonstrated that this significantly augments the burn rate. When such a term is not considered, the 1-D predictions deviate by more than 15% from the direct numerical 3-D simulations. In the HMX–HTPB simulations reported here, the lack of a model for the HTPB melting can be one of the factors that leads to the overprediction of the burn rate shown in Figs. 14 and 15.

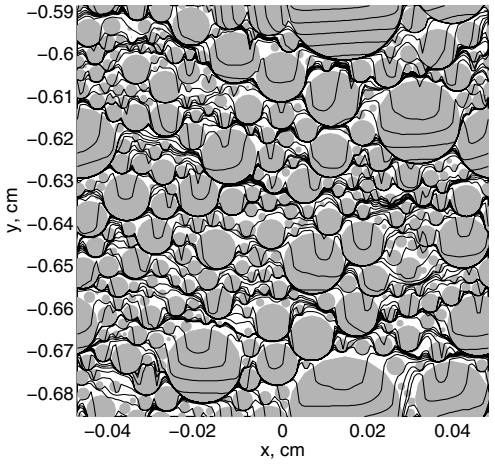

Fig. 16 Time history of the surface location for pack A at 68 atm; time lag between levels is 3×10^{-3} s; two-dimensional slice of the pack that corresponds to cut 8 in Fig. 10.

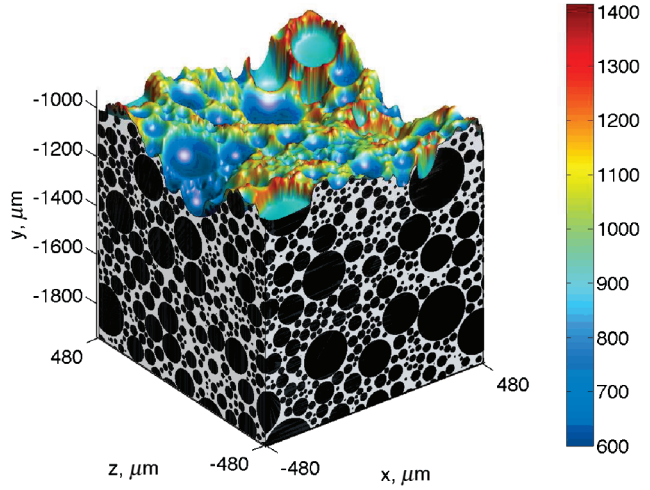

a) Time: 205 ms

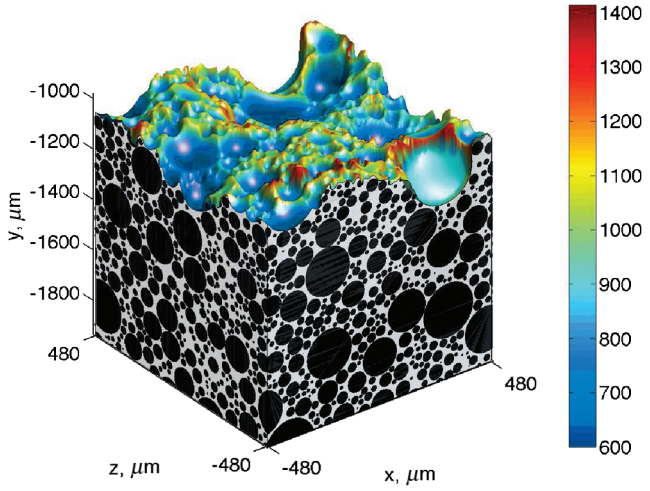

b) Time: 215 ms

Fig. 17 Surface temperature and corrugated interface for pack A, model 3, at 68 atm.

Surface corrugation is caused by the difference in the burning speeds of the two ingredients. The burn rate of pure HMX is significantly larger than the binder burn rate, which makes the deflagration an intermittent process. A burning-rate color map for the propellant surface at different times is shown in Fig. 18. The figure refers to pack B, model 3, at 40 atm. Each panel corresponds to a different time of the deflagration; the time lag between consecutive panels is 4 ms. The figure highlights the difference in deflagration speed between the oxidizer and binder. It also shows that locally, the HMX burns close to the 1-D steady rate for that pressure. Figure 19 shows a comparison of the surface-averaged burning-rate time traces for pack A at the three pressures considered and demonstrates that the irregularity in burning is augmented by an increased pressure.

VII. Conclusions

A numerical framework for the simulation of 3-D HMX–HTPB composite propellant combustion is presented. The analysis centers around the determination of global (false) kinetic models suitable for simulation of multidimensional randomly packed propellant. The

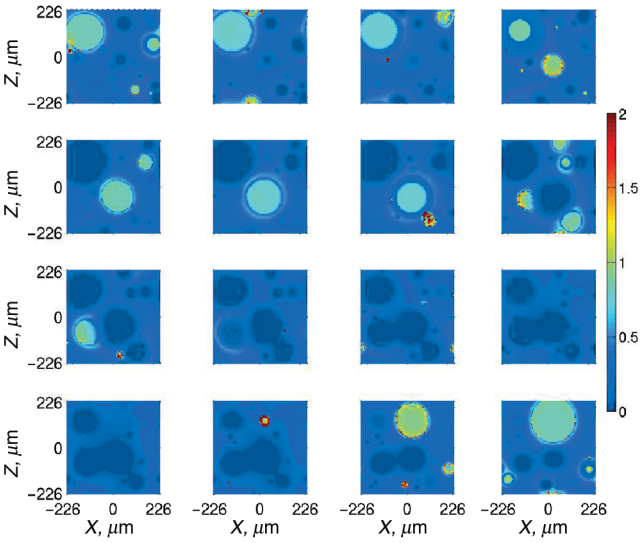

Fig. 18 Burn-rate distribution for pack B, model 3, at 40 atm; each panel refers to a different time; time lag between consecutive frames is 4 ms.

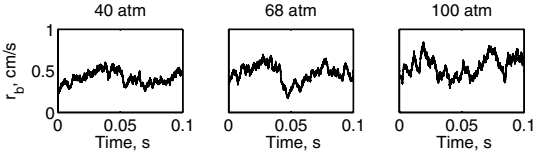

Fig. 19 Time history of the surface-averaged burn rate for pack A, model 3; time interval of 0.1 s is representative of the pack burn-through time and, at 68 atm, corresponds to 460 μm of burning (approximately half of the pack period).

proposed approach involves global optimization of model results against a set of burning characteristics measured in 1-D steady combustion conditions. A genetic algorithm is used to maximize an objective function containing up to 18 parameters and determined as the deviation of the predicted burning characteristics from experiments. The optimization technique is flexible, computationally inexpensive, and does not require detailed knowledge of the reaction paths in the gas and condensed phases; thus, the method is applicable to a large class of propellants.

Three models of increasing complexity are considered in this research; all are optimal design points given the underlying set of performance measures, burning characteristics, and design parameters. For the first model, the one-dimensional calibration reveals that to match blend burn rates, the diffusion-flame reactions must be strong. Such heterogeneous reactions are supported by the HMX–HTPB vapors, act to decrease the gas temperatures close to the surface, and result in decreasing the burn rate when the fuel content is increased.

Experimental and detailed chemistry evidence suggest that the strength of the endothermic reaction associated with the secondary diffusion flame is nonphysical (an outcome of the simplified chemistry modeling); such a reaction is therefore neglected in model 2, with the goal of demonstrating its importance within the BDP [14] model.

The difficulty associated with matching blend burn rates is circumvented in model 3 by hypothesizing that the presence of the HTPB gas in the oxidizer stream reduces the chemical energetic contribution of HMX decomposition, not only by reducing the temperature at which reaction occurs, but also by inhibiting the reaction itself, thus providing an anticatalytic effect. On the other hand, model 2 is obtained with a strategy similar to that in model 1, but the secondary diffusion flame is neglected to demonstrate its necessity.

The ability of the models to predict burning characteristics of realistic (randomly packed and heterogeneous) propellants is demonstrated by carrying out a multidimensional analysis using two periodic pack samples with different particle distributions. Comparing predicted time–space-integrated burn-rate data and experiments shows that both models 1 and 2 yield poor results, with model 1 predicting quenching of the sample. Model 3 gives results in satisfactory agreement with experiments with errors around 20%. Therefore, the simulations demonstrate the ability of the optimization strategy to produce accurate chemistry models once an appropriate reaction framework is deduced.

Acknowledgments

This work was supported by the U.S. Department of Energy through the University of California under subcontract B523819. J. D. Buckmaster was also supported by the U.S. Air Force Office of Scientific Research. The authors would like to thank Richard Yetter and Merril Beckstead for the stimulating discussions.

References

[1] Massa, L., Buckmaster, J., and Jackson, T. L., "Recent Developments in the Modeling of Heterogeneous Propellant Combustion," AIAA Paper 2005-4467, July 2005.

[2] Jackson, T. L., and Buckmaster, J., "Heterogeneous Propellant Combustion," *AIAA Journal*, Vol. 40, No. 6, 2002, pp. 1122–1130.

[3] Beckstead, M. W., and McCarty, K. P., "Modeling Calculations for HMX Composite Propellants," *AIAA Journal*, Vol. 20, No. 1, 1982, pp. 106–115.

[4] Vyazovkin, S., and Wight, C. A., "Kinetics in Solids," *Annual Review of Physical Chemistry*, Vol. 48, 1997, pp. 125–149.

[5] Miller, M. S., and Anderson, W. R., "Energetic-material Combustion Modelling with Elementary Gas-Phase Reactions: A Practical Approach," *Solid Propellant Chemistry, Combustion and Motor Interior Ballistics*, edited by V. Yang, T. Brill, and W.-Z. Ren, Vol. 185, AIAA, New York, 2000, pp. 501–531.

[6] Brewster, M. Q., "Solid Propellant Combustion Response: Quasi-Steady (QSHOD) Theory Development and Validation," *Solid Propellant Chemistry, Combustion and Motor Interior Ballistics*, edited by V. Yang, T. Brill, and W.-Z. Ren, Vol. 185, AIAA, New York, 2000, pp. 607–637.

[7] Massa, L., Jackson, T. L., and Buckmaster, J., "Optimization of Global Kinetics Parameters for Heterogeneous Propellant Combustion Using a Genetic Algorithm," *Combustion Theory and Modelling*, Vol. 11, No. 4, Aug. 2007, pp. 1–16.

[8] Miller, M. S., "In Search of an Idealized Model of Homogeneous Solid Propellant Combustion," *Combustion and Flame*, Vol. 46, No. 1, 1982, pp. 51–73.

[9] Ben-Reuven, M., and Caveny, L. H., "Nitramine Flame Chemistry and Deflagration Interpreted in Terms of a Flame Model," *AIAA Journal*, Vol. 19, No. 10, 1979, pp. 1276–1285.

[10] Ward, M. J., Brewster, M. Q., and Son, S. F., "Steady Deflagration of HMX with Simple Kinetics—A New Modeling Paradigm," AIAA Paper 1997-590, Jan. 1997.

[11] Mitani, T., and Williams, F. A., "A Model for the Deflagration of Nitramines," *Proceedings of the 21st Symposium (International) on Combustion*, Combustion Inst., Pittsburgh, PA, 1986, pp. 1965–1974.

[12] Price, C. F., Boggs, T. L., and Derr, R. L., "The Steady State Combustion of Ammonium Perchlorate and Cyclotetramethylenetetranitramine," AIAA Paper 1979-164, Jan. 1979.

[13] Burg, C., and Newman, J., "Computationally Efficient, Numerically Exact Design Space Derivatives via the Complex Taylor's Series Expansion Method," *Computers and Fluids*, Vol. 32, No. 3, Mar. 2003, pp. 373–383.

[14] Beckstead, M. W., Derr, R. L., and Price, C. F., "Model of Composite Solid-Propellant Combustion Based on Multiple Flames," *AIAA Journal*, Vol. 8, No. 12, 1970, pp. 2200–2207.

[15] Lengelle, G., "Thermal Degradation Kinetics and Surface Pyrolysis of Vinyl Polymers," *AIAA Journal*, Vol. 8, No. 11, 1970, pp. 1989–1996.

[16] Lengelle, G., "Combustion Mechanisms of Nitramine-Based Propellants with Additives," *Journal of Propulsion and Power*, Vol. 6, No. 6, 1990, pp. 718–726.

[17] Esker, D. R., and Brewster, M. Q., "Laser Pyrolysis of Hydroxyl-Terminated Polybutadiene," *Journal of Propulsion and Power*, Vol. 12, No. 2, 1996, pp. 296–301.

[18] Cohen, N. S., Fleming, R. W., and Derr, R. L., "Role of Binders in Solid Propellant Combustion," *AIAA Journal*, Vol. 12, No. 2, 1974, pp. 212–218.

[19] Davidson, J. E., and Beckstead, M. W., "A Three-Phase Model of HMX Combustion," *Proceedings of the 26th Symposium (International) on Combustion*, Combustion Inst., Pittsburgh, PA, 1996, pp. 1989–1996.

[20] Prasad, R., Yetter, R. A., and Smooke, M. D., "An Eigenvalue Method for Computing the Burning Rates of HMX Propellants," *Combustion and Flame*, Vol. 115, No. 3, Nov. 1998, pp. 406–416.

[21] Zenin, A., "HMX and RDX: Combustion Mechanism and Influence on Modern Double Base Propellant," *Journal of Propulsion and Power*, Vol. 11, No. 4, 1995, pp. 752–759.

[22] Lengelle, G., "Physico-Chemical Mechanism of Solid Propellant Combustion," *Solid Propellant Chemistry, Combustion and Motor Interior Ballistics*, edited by V. Yang, T. Brill, and W.-Z. Ren, Vol. 185, AIAA, New York, 2000, pp. 287–334.

[23] Zel'dovich, Y. B., "On the Combustion Theory of Powders and Explosives," *Journal of Experimental and Theoretical Physics*, Vol. 12, 1942, pp. 498–510 (in Russian).

[24] Chen, M., Buckmaster, J. D., Jackson, T. L., and Massa, L., "Homogenization Issues and the Combustion of Heterogeneous Solid Propellants," *Proceedings of the 29th Symposium (International) on Combustion*, Combustion Inst., Pittsburgh, PA, 2002, pp. 2923–2929.

[25] Beckstead, M. W., Puduppakkam, K., and Yang, V., "Modeling and Simulation of Combustion of Solid Propellant Ingredients Using Detailed Chemical Kinetics," AIAA Paper 2004-4036, July 2004.

[26] Finlinson, J. C., Stalnaker, R., and Blomshield, F. S., "HMX and RDX T-Burner Pressure Coupled Response from 200 to 1000 psi," AIAA Paper 1998-556, Jan. 1998.

[27] Atwood, A. I., Boggs, T. L., Curran, P. O., Parr, T. P., and Hanson-Parr, D. M., "Burning Rate of Solid Propellant Ingredients, Part 1: Pressure and Initial Temperature Effects," *Journal of Propulsion and Power*, Vol. 15, No. 6, 1999, pp. 740–747.

[28] Zenin, A., Finjakov, S. V., Puchov, V. M., and Ibragimov, N. G., "Temperature and Pressure Sensitivities of Burning Wave Parameters of Nitramine-Containing Propellants and HMX," *Journal of Propulsion and Power*, Vol. 15, No. 6, 1999, pp. 753–758.

[29] Kochevets, S., Buckmaster, J. D., Jackson, T. L., and Hegab, A., "Random Packs and Their Use in the Modeling of Heterogeneous Solid Propellant Combustion," *Journal of Propulsion and Power*, Vol. 17, No. 4, 2001, pp. 883–891.

[30] Knott, G. M., Jackson, T. L., and Buckmaster, J., "The Random Packing of Heterogeneous Propellants," *AIAA Journal*, Vol. 39, No. 4, 2001,

pp. 678–686.
[31] Massa, L., Jackson, T. L., Buckmaster, J., and Campbell, M., "Three-Dimensional Heterogeneous Propellant Combustion," *Proceedings of the 29th Symposium (International) on Combustion*, Combustion Inst., Pittsburgh, PA,2002, pp. 2975–2983.
[32] Massa, L., Jackson, T. L., and Short, M., "Numerical Simulation of Three-Dimensional Heterogeneous Propellant," *Combustion Theory and Modeling*, Vol. 7, No. 3, 2003, pp. 579–602.
[33] Massa, L., Jackson, T. L., and Buckmaster, J., "Using Heterogeneous Propellant Burning Simulations as Subgrid Components of Rocket Simulations," *AIAA Journal*, Vol. 42, No. 9, 2005, pp. 1889–1900.

C. Kaplan
Associate Editor